NASA-CR-163098
19800024842

NASA Contractor Report 163098

FLOW VISUALIZATION STUDY OF THE F-14 FIGHTER AIRCRAFT CONFIGURATION

Dale J. Lorincz

Contract NAS4-2616
September 1980

NASA Contractor Report 163098

FLOW VISUALIZATION STUDY OF THE F-14 FIGHTER AIRCRAFT CONFIGURATION

Dale J. Lorincz
Northrop Corporation

Prepared for
Dryden Flight Research Center
under Contract NAS4-2616

National Aeronautics and
Space Administration
1980

Intentionally Left Blank

CONTENTS

FLOW VISUALIZATION STUDY OF THE F-14 FIGHTER AIRCRAFT CONFIGURATION

By
Dale J. Lorincz
Northrop Corporation, Aircraft Division
Hawthorne, California

SUMMARY

Water tunnel studies have been performed to qualitatively define the flow field of the F-14. Particular emphasis was placed on defining the vortex flows generated at high angles of attack. The flow visualization investigation was conducted in the Northrop water tunnel using a 1/72-scale model of the F-14 with the wing leading edge swept to 20°. Flow visualization photographs were obtained over an angle of attack range of from 5° to 55° at sideslip angles of 0° and 10°.

The F-14 model was investigated to determine, in detail, the vortex flow field development, vortex path, and vortex breakdown characteristics as a function of angle of attack and sideslip. Vortex flows were found to develop on the highly swept glove and on the upper surface of the forebody. The mapping of these flows was done to assist NASA DFRC in planning future studies on the full-scale aircraft and to aid in interpretation of past flight test and wind tunnel results.

Tests were performed to determine the changes in the glove vortex flow field with 10° of sideslip. The windward vortex shifted inboard toward the windward vertical tail and broke down farther forward than the leeward vortex. This asymmetric breakdown of the vortices in sideslip contributes to the reduction in lateral stability that occurs above 20° angle of attack. The initial loss of directional stability of the aircraft is a consequence of the adverse sidewash from the windward vortex and the reduced dynamic pressure at the vertical tails which were observed in the water tunnel.

Asymmetries in the vortex system generated by the forebody were observed in the water tunnel at zero sideslip and high angles of attack. A large nose boom was added to the forebody, and it was found to shed a turbulent wake which reduced the vortex asymmetry. The orientation of the forebody vortex system in sideslip which was observed in these tests would generate a destabilizing yawing moment throughout the high angle of attack range.

INTRODUCTION

The flow field around an aircraft such as the F-14 at high angles of attack is three dimensional and very complex. This flow field typically consists of regions of separated, low-energy flow and concentrated vortex flows of high energy. From the results of past investigations (References 1, 2, and 3), it is known that this complex flow produces aerodynamic characteristics which are highly nonlinear in angle of attack and/or sideslip.

A more complete understanding of the flow fields on the wing, the glove, and the fuselage forebody of the F-14 and how they influence aerodynamic characteristics can be obtained through flow visualization. Details of the vortex flow field development, vortex path, and vortex breakdown characteristics as a function of angle of attack and sideslip are desired. The mapping of the vortex flows will identify areas of interest for pressure instrumentation to be used on the full-scale aircraft in future flight tests being considered by NASA DFRC.

Studies done at Northrop using a water tunnel have provided excellent visualization of vortex flows on wings and fuselage forebodies. The water tunnel has been used to qualitatively define the vortex flow fields on many aircraft configurations. All testing for this study was done in the Northrop diagnostic water tunnel which has a test section of 0.41 by 0.61 meters. Changes in angle of attack, sideslip, and model configuration can be made quickly and inexpensively using small scale models. The flow visualization results discussed in this report were obtained using a 1/72-scale model of the F-14. The angle of attack was varied from 5° to 55° at sideslip angles of 0° and 10°.

The primary purpose of these tests was to define the vortex flow fields generated above the glove and on the fuselage forebody. The sensitivity of these vortex flows to changes in angle of attack and sideslip was determined. The effect of a flight test nose boom on the forebody vortex pair was investigated. Wherever possible, the water tunnel results are compared to wind tunnel data obtained in the 12-foot pressure tunnel at NASA Ames Research Center on a 1/16-scale F-14 model.

SYMBOLS

C_ℓ	rolling moment coefficient
C_N	normal force coefficient
C_n	yawing moment coefficient
M	Mach number
$\dot{m}_I$	mass flow to inlet
$\dot{m}_\infty$	capture mass flow
α	angle of attack
β	angle of sideslip
Λ	leading-edge sweep angle

EXPERIMENTAL METHODS

Water Tunnel Facility

The Northrop water tunnel is a closed return tunnel used for high quality flow visualization of complex three-dimensional flow fields. The water tunnel is shown schematically in Figure 1. The test section is 0.41 m by 0.61 m by 1.83 m long and has walls made of transparent Plexiglas. The test section is oriented in the vertical direction, which permits the model to be viewed from any angle. A model is shown installed in the test section in Figure 2. The model is accessed through the top of the tunnel by means of suspension cables connected to the model support system.

The model support system consists of a sting and sideslip arc which is capable of pitch angles from -10° to 70°, concurrent with a sideslip range of -20° to 20°. The sideslip angle is fixed prior to the model installation. The pitch angle is then manually adjusted from the side of the test section.

Test Procedure

The flow visualization in the water tunnel is obtained by injection of colored food dyes having the same density as water. The density of water is 800 times that of air, which gives the dye excellent light reflecting characteristics relative to using smoke in air. The dye is introduced into the flow field through small orifices and dye tubes distributed along the body of the model. The dye can also be introduced through a dye probe which can be accurately positioned at any point in the test section by means of a traversing mechanism.

Inlet flows are simulated in the water tunnel by applying suction to tubes connected to the rear of the model's exhaust nozzles. The tubes are run to a water flow meter outside the tunnel. The flow meter is used to accurately measure and set the inlet flow rate. The water tunnel is operated at a test section velocity of 0.1 meters/second which has been found to produce the best flow visualization results. This velocity corresponds to a Reynolds number of 1×10^5/meter.

VORTEX FLOW FIELDS

Prior to development of the Northrop water tunnel, the question of whether vortex flow fields in air could be properly simulated in water with sufficient accuracy was considered. It is well known that if cavitation is avoided and compressibility effects are negligible, then the fluid motions of water and air at the same Reynolds number are dynamically similar. For identical model scale and velocity, the Reynolds number in water is higher by a factor of 15. However, because of practical limitations in speed and model scale, water tunnel tests are generally run at Reynolds numbers well below those of wind tunnels.

For thin, swept wings, boundary layer separation occurs along the sharp leading edge. The sheet of distributed vorticity that is shed rolls up into a spiral vortex with a concentrated core. A laminar separation will occur at the sharp leading edge of the wing at the Reynolds numbers encountered in flight and in the water tunnel. The vortex generation is therefore not sensitive to Reynolds number and the vortex formed in the water tunnel is representative of flight (References 4, 5, and 6).

Once the leading-edge vortex flow has formed, its stability can be affected by external conditions. At high angles of attack, the vortex core can undergo a sudden expansion, which is referred to as vortex breakdown or burst. Above the stalled portion of a wing and at the wing trailing edge, there is a large adverse pressure gradient. This negative velocity gradient will reduce the axial velocity within the core of the vortex. The vortex will then burst with a rapid expansion to a larger, slower rotating flow. The breakdown of the vortex core depends on the magnitude of the rotational and axial velocities, the external pressure gradient, and the degree of flow divergence. Studies of vortex stability have shown that the external pressure gradient is a dominant parameter for vortex burst. Therefore, when a leading-edge vortex encounters a large adverse pressure gradient above a wing, it will break down in a similar manner in the water tunnel as in the wind tunnel and in flight.

The rolled-up vortex sheet induces large suction pressures on the upper surface of the wing which produce additional lift. An increase in the rotational velocity of the vortex will induce lower pressures on the surface and increase the vortex lift. At the same time, an increase in rotational velocity decreases the stability of the vortex, making it more likely to burst. A moderate increase in the axial velocity of a vortex will increase the stability of the vortex and delay any breakdown.

The influence of Reynolds number on the vortex breakdown position has been investigated at Northrop and by others. In the Northrop studies (Reference 4), the angle of attack at which vortex breakdown occurred at the trailing edge was observed on delta wings having leading-edge sweep angles of 55° to 85°. Figure 3, which is taken from Reference 4, shows that the results obtained in the Northrop water tunnels fall within the range of angles of attack observed by others. The data shown include results from other water tunnels as well as wind tunnels and covers the Reynolds number range of 10^4 to 10^6, based on root chord. Note that the variation in the data due to Reynolds number is no greater than the variation associated with different facilities and different flow visualization techniques at the same Reynolds number. All of the data follow the same trend of increasing angle of attack for vortex breakdown at the trailing edge as the leading-edge sweep angle is increased.

The vortex burst locations above the upper surface of thin, swept wings in the water tunnel are in good agreement with the results at higher Reynolds numbers in wind tunnels at moderate to high angles of attack because the external pressure

gradient is the dominant effect. Surface flows at low angles of attack that are not yet vortex dominated can be more sensitive to Reynolds number effects. In the water tunnel, early laminar separation can occur on leading-edge flaps and slats. Slats would delay flow separation over a wing to a higher angle of attack when tested at a high Reynolds number.

The asymmetric shedding of the vortex pair which forms on an aircraft forebody at zero sideslip and high angles of attack is associated in part with an inviscid hydrodynamic instability. The water tunnel studies generally show good agreement of the observed onset of the forebody vortex asymmetry with wind tunnel measurements of the asymmetric side force. The orientation of the forebody vortex system in sideslip has been found to correspond with the directional stability characteristics at high angles of attack of several fighter configurations. A side force is produced toward the forebody vortex which remains closest to the surface in sideslip.

MODEL DESCRIPTION

The water tunnel flow visualization studies were conducted with a 1/72-scale model of the F-14. A three-view drawing of the model is shown in Figure 4. The model configuration tested was with the landing gear up and all control surfaces at zero deflection. The wing was in the full-forward position with a leading-edge sweep of 20°. The wing was tested in the clean configuration with the slat undeflected and no trailing-edge flap deflection.

The model was built with flow-through ducts from the inlets to the exhaust nozzles. To provide the desired inlet mass flow rate, a suction tube was connected to each exhaust nozzle with no change in the external lines. The model support sting was installed between the suction tubes on the lower surface of the model. The inlet mass flow ratio was set to simulate the inlet conditions at a freestream Mach number of 0.3. This mass flow ratio at zero angle of attack is $\dot{m}_I/\dot{m}_\infty = 1.19$. The mass flow would be pulled in from an area larger than the capture area of the inlet.

In order to visualize the flow field, the model was equipped with dye injection orifices. Great care was taken in locating the dye orifices to insure that dye introduced into the external flow would be entrained into the vortices. A traversing dye probe was used to survey the model to find the exact location for each orifice. On the forebody, the orifices were distributed along the windward side and were installed flush with the surface. A dye orifice was placed in the leading edge of the wing near the wing-glove junction. For dye to be entrained into the vortex which forms above the glove, a dye orifice was placed in the leading edge of the glove at a point aft and outboard of the apex. A dye orifice was also located flush to the lower surface of the inlet cowl near the outboard corner.

RESULTS AND DISCUSSION

The experimental results that were obtained from the water tunnel flow visualization studies consist of a set of photographs documenting the flow field of the F-14. Selected results are referred to in the text and are given at the end of this report. Whenever appropriate, comparisons are made between the water tunnel flow visualization results and wind tunnel force and moment data. The wind tunnel data are for a 1/16-scale F-14 model in the clean configuration. The data were obtained in the 12-foot pressure tunnel at the NASA Ames Research Center and are presented in Reference 7.

Wing-Glove Flow Field Characteristics

The flow field of the wing and the glove for the clean configuration at zero sideslip is presented in Figure 5. The dye orifice in the leading edge of the glove and at the outboard corner of the inlet cowl are located such that the dye from them would be entrained into a vortex. No vortex is formed on the wing because of the low leading-edge sweep of 20°. At 8° angle of attack, a vortex begins to form on the glove. The vortex is rather weak and diffuse. A weak vortex is also beginning to form at the outboard edge of the inlet cowl. It is inboard of the glove vortex and moves straight aft where it passes above the horizontal tail.

With an increase in angle of attack to 10°, both the glove and the inlet vortex are better defined as shown in

Figure 5. An increase in strength of both the vortices is indicated by the increase in the rotational velocity that was observed. The inlet vortex appears to be the weaker of the two since it is swept underneath the glove vortex and then becomes entrained. The dye from the leading edge of the wing is drawn up and over the top of the glove vortex. In the profile view of Figure 5, the flow is seen to separate near the leading edge of the wing. The use of slats on the aircraft in flight would make the stall progression much more gradual on the wing panel. Maintaining attached flow and low pressure over the wing should shift the vortex breakdown to farther outboard.

By 15° angle of attack, the inlet and glove vortices have combined into a single vortex. The vortex begins along the outboard edge of the inlet cowl, while the flow that separates at the leading edge of the glove forms a feeding sheet to the same vortex. The vortex above the glove is now tightly rolled up, and it continues to breakdown near the wing trailing edge. At 17° angle of attack, however, the burst point of the glove vortex is farther forward. This is very evident in the profile view of Figure 5 where the sudden expansion of the vortex at breakdown is seen to be farther forward.

Between 20° and 25° angle of attack, the burst point of the glove vortex continues to move forward. The vortex becomes more diffuse and unsteady with increasing angle of attack. When the flow separates at the sharp lip of the inlet, there is a large area of turbulent, separated flow on the upper surface of the inlet cowl. This turbulent flow adjacent to the glove vortex contributes to the unsteadiness observed in the vortex. Also with increasing angle of attack, flow is spilled around the side wall of the inlet. The side wall has a sharp leading edge and flow separation occurs. The separated, turbulent flow on the side wall of the inlet moves aft and some goes over the glove disturbing the vortex. When the inlet mass flow rate was reduced, more flow would be spilled, and increased unsteadiness was seen in the vortex.

Despite the diffuse nature of the flow above the glove, there was still some rotation to the flow at 30° angle of attack. It does not persist far downstream as the glove itself is becoming stalled with some reversed flow seen on the surface. By 35° angle of attack, the glove vortex has been replaced by a turbulent wake which extends across the glove, the upper surface of the inlet cowl, and most of the aft fuselage. The wake does not extend into the region directly behind the canopy.

Figure 6 presents the normal force coefficients as a function of angle of attack for the clean configuration

at low speeds. This curve was obtained from data on a 1/16-scale model tested in the 12-foot pressure tunnel at the NASA Ames Research Center. A linear, low angle of attack regime was identified in Reference 7 where the normal force undergoes a steep rise. The beginning of the vortex flow regime is given as being 9° angle of attack. In the water tunnel, the glove and inlet vortex were seen to have begun to form at 9° angle of attack. The vortex flow on the glove produces a continued rise in normal force until 30° angle of attack. The end of the vortex flow regime at 30° angle of attack corresponds to the flow above the glove becoming diffuse and unsteady with little rotation as observed in the water tunnel at 30° angle of attack. For angles of attack above 30°, the normal force remains fairly constant. In the water tunnel, a separated wake was seen to extend across the inlet cowl and glove at 35° and higher angles of attack. The forebody and area aft of the canopy are free of the wake because of a vortex pair that forms on the forebody which is discussed in a later section of this report.

Wing-Glove Flow Field in Sideslip

The sensitivity of the wing-glove flow field to an angle of sideslip was investigated. The model was set at 10° sideslip angle and the angle of attack was varied from 8° to 35°. Photographs of the wing-glove flow field at 10° of sideslip are presented in Figure 7.

At both 8° and 10° angle of attack, the weak inlet vortex on the leeward side has shifted outboard and a single vortex is formed above the leeward glove. On the windward side, a separate inlet and glove vortex are formed, but they combine before reaching the trailing edge of the wing. Both glove vortices have shifted toward the leeward side. This brings the windward vortex closer to the windward tail.

The vortex emanating from the windward inlet at 15° angle of attack is much stronger than the glove vortex which forms closer to the leading edge of the glove. The glove vortex merges with the inlet vortex after a short distance. The windward inlet vortex is more tightly rolled up than the vortex seen at zero sideslip in Figure 5. It is also breaking down farther forward in sideslip. On the windward side, the sweep angle is effectively reduced. This reduces the stability of the vortex, causing it to burst farther forward. The rotational velocity of the windward vortex was observed to be increased. This is indicative of an increase in vortex

strength which increases the vortex lift on the windward side compared to the vortex lift on the glove at zero sideslip. This has been observed in the pressure measurements made on a delta wing in Reference 8. The velocity component normal to the leading edge of both the wing and the glove is greater on the windward side, which will also increase the lift.

In Figure 7 at 17° angle of attack, the leeward vortex is seen to burst farther aft than the vortex at zero sideslip in Figure 5. The leeward side is at an effectively higher sweep angle in sideslip. This higher sweep increases the vortex stability, while reducing the vortex strength. The increased stability will slow the forward progression of the vortex burst. The decrease in vortex strength will reduce the vortex lift on the leeward side (Reference 8).

The increased lift on the windward wing and glove contribute to a stable rolling moment in sideslip. The breakdown of windward vortex is seen in Figure 7 to move forward with increasing angle of attack faster than on the leeward side. This will begin to reduce the stable rolling moment. At 30° angle of attack, the windward glove is close to stall while a vortex is still present on the leeward side. This early stall of the windward side will reduce the stable rolling moment even farther.

At 17° angle of attack, Figure 7 shows that the burst of the windward vortex is ahead of the windward vertical tail. Aft of the vortex burst, there is some rotational motion, but the velocities are much lower than in the vortex prior to breakdown. In the profile view of Figure 7, the wake from the burst vortex is seen to extend above the top of the vertical tail. The dynamic pressure at the windward vertical tail is reduced because the low velocity wake of the burst vortex impinges on it and because both vertical tails are shielded from the freestream flow by the wing and the fuselage.

The rotating vortices can induce a sidewash in the vicinity of the vertical tails. A dye probe was placed at several locations across the fuselage to determine the flow direction near the surface. The results of this survey for the model at 20° angle of attack and 10° of sideslip are given in Figure 8. The vortex on the windward side is closer to the vertical tail and the angle of induced outboard flow is greater than on the leeward side. The direction of the flow beneath the vortex is no longer toward the fuselage centerline as was the case at low angles of attack. The windward vortex thus induces a strong "adverse" sidewash at high angles of attack. Above the windward vortex, the sidewash is in a stabilizing direction but with the tapered vertical tail there is less area

toward the tip for it to act on. The leeward vortex induces a favorable sidewash on the surface ahead of the leeward vertical tail. The leeward vortex moves away from the vertical tail in sideslip, and the angle of the sidewash is seen in Figure 8 to be less than on the windward side.

Figure 9 presents the rolling moments and yawing moments as a function of angle of attack for the clean configuration at 10° of sideslip. These curves, given in Reference 7, were obtained from data on a 1/16-scale model tested in the 12-foot pressure tunnel at the NASA Ames Research Center. As the angle of attack is increased, there is a reduction in the dynamic pressure at the vertical tails as they become shielded by the fuselage and immersed in the low-velocity wake of the burst windward vortex. The resulting reduction in yawing moment with increasing angle of attack is evident in Figure 9. Above approximately 17° angle of attack, the model is unstable directionally. The adverse sidewash ahead of the windward vertical tail is an additional destabilizing factor. For the twin-tailed fighter model investigated in Reference 3, the adverse sidewash was strong enough to cause the vertical tails to actually be destabilizing at high angles of attack. For angles of attack of 30° and higher, the yawing moments in sideslip can be influenced by the vortex pair on the forebody and the forebody cross-sectional shape (Reference 9).

The more forward breakdown of the windward vortex compared to the leeward vortex would tend to limit the stable rolling moment that is produced in sideslip. In Figure 9 the rolling moment is seen to decrease with increasing angle of attack from 25° to 30°. In the water tunnel, the largest asymmetry in burst points between the windward and leeward vortices was seen in this angle of attack range. The windward vortex becomes completely burst while a vortex is still formed on the leeward side. At 35° angle of attack, where both vortices have burst at the apex of the glove, the rolling moment is seen in Figure 9 to again be increasing with increasing angle of attack.

Forebody Flow Field Characteristics

The flow field of the forebody of the F-14 at zero sideslip and selected angles of attack is presented in both plan and profile views in Figure 10. No vortex flow is evident at 20° angle of attack. The dye being injected from the underside of the fuselage is seen to move upward around the lower corner of the forebody, then turn aft, and separate at the rear of the canopy. There is some rotation in the wake aft

of the canopy at 25° angle of attack before the flow becomes turbulent. With increasing angle of attack, the crossflow over the forebody sweeps the boundary layer to the upper surface where it separates and rolls up into a symmetric vortex pair. The rotating helical pattern of the vortex is first seen in Figure 10 at 30° angle of attack. With increasing angle of attack, the rotational velocity of the vortex and therefore its strength is increased. The rotating helical pattern of the vortex is better defined at 35° angle of attack.

In the profile views of Figure 10, it is seen that at 30° and 35° angles of attack, the forebody vortices are turned downward over the rear of the canopy and are breaking down when they reach the upper surface of the fuselage. At the higher angles of attack in Figure 10, the vortices are seen to burst above the fuselage surface and before reaching the vertical tails. Above the stalled wing and fuselage is a large increasing or adverse pressure gradient which will decelerate the axial velocity within the core of the vortex. The vortex will then burst with a rapid expansion to a larger, slower rotating, turbulent flow.

The vortex pair above the forebody develops an asymmetry with increasing angle of attack. At 50° angle of attack and zero sideslip, the right side vortex has shifted upward, away from the surface. The vortex on the left side remains close to the body. The vortex asymmetry becomes more pronounced by 55° angle of attack, and it is clearly seen in the profile view of Figure 10. The height of the right side vortex above the surface and above the left vortex is increased, and a shift to the right in the lateral position of the vortex pair can be seen in the plan view of Figure 10.

The resultant force generated by the forebody will be rotated to one side as a result of the shift in the position of the forebody vortices (Reference 1). The vortex which remains closest to the surface of the forebody will exert a larger suction pressure than the one that has moved upward. The reduced influence of the high vortex and the induced suction of the low vortex will change the circumferential pressure distribution over the entire forebody. This produces a net side force toward that side of the forebody on which the vortex is closest (Reference 10). This side force on the forebody will cause asymmetric yawing moments at zero sideslip and high angles of attack. It is stated in Reference 7 that during the tests of the F-14 in the 12-foot pressure tunnel at the NASA Ames Research Center, large values of yawing moment could be measured at zero sideslip at around an angle of attack of 55°.

The forebody vortices are known to exist to as high as 80° angle of attack (Reference 11), but the affected surface area becomes smaller. At 55° angle of attack, the vortices are turning streamwise above the canopy and are farther from the surface. The flow is not fully separated on the upper surface of the aircraft until 70° to 80° angle of attack when the forebody vortices are replaced by a 2-D type separation with a periodic shedding of the wake.

During the flight testing of the F-14 at the NASA Dryden Flight Research Center, a large instrumentation nose boom is used. The nose boom carries flight test instrumentation to determine airspeed, altitude, angle of attack, and sideslip. Figure 11 illustrates the effect of the nose boom on the forebody at zero sideslip. At angles of attack below 35°, little change in the forebody flow field is observed. At 40° angle of attack a change in the forebody flow field is evident when compared to the forebody without the nose boom in Figure 10. The forebody vortex pair is more diffuse, with greater turbulence, and there is some mixing between the two vortices. Through the use of a traversing dye probe, it was possible to see that the boom sheds a periodic wake which passes near enough to the forebody vortex pair to cause a disturbance. The alternating vortices that are shed and move downstream from the boom are responsible for the alternating pattern seen in the plan view of Figure 11 at 40° and higher angles of attack. This alternating mixing between the forebody vortices occurs at the same frequency as the vortex shedding from the nose boom. The wake from the nose boom reduces the asymmetry in the vortex flow field at 55° angle of attack that occurred on the clean forebody. A nose boom mounted on a 3.5 fineness ratio tangent ogive forebody was shown in Reference 12 to greatly reduce the large side forces at zero sideslip.

The flow field around the forebody at 10° of sideslip with the nose boom in place is presented in Figure 12. In the plan views of Figure 12, a shift in the vortex pair toward the leeward side is evident when compared to the symmetrical pattern seen at zero sideslip in Figure 11. In the profile views of Figure 12, the windward vortex is seen to have shifted in sideslip to a position higher up on the side of the fuselage and closer to the fuselage centerline. The leeward vortex is positioned closer to the side of the fuselage. A vortex is seen in Figure 12 aft of the canopy on the windward side at 20° angle of attack. This vortex moves aft above the fuselage until it breaks down near the end of the fuselage. A vortex is seen on the leeward side at 25° angle of attack, but it appears to be weaker than the windward vortex. The leeward vortex is closer to the side of the forebody and closer to the upper fuselage surface. The leeward vortex breaks down

before reaching the end of the fuselage. At the angle of attack of 30°, the windward glove is nearly stalled as seen in Figure 7. The separated flow above the glove and the fuselage on the windward side causes the windward forebody vortex to break down farther forward at 30° angle of attack. When the angle of attack is increased to 35° angle of attack and above, the orientation of the vortices is seen to be similar to that at the lower angles. The windward vortex remains farthest from the surface while the leeward vortex remains close to the side of the fuselage.

Comparing the leeward and windward profile views of Figure 12, the boundary layer separation line is seen to shift in sideslip to a position lower on the leeward side and higher on the windward side. This indicates a shift in the stagnation line on the lower surface. The flow was seen to separate downstream of the gun mounted in the forward fuselage which is on the leeward side in Figure 12.

At low angles of attack, the forebody is directionally destabilizing because of its side area ahead of the center of gravity. At higher angles of attack, the forebody vortex pair which forms will affect the directional stability of the aircraft. This results primarily from the vortices producing a side force on the forebody itself rather than an interaction with the vertical tails (Reference 9). Whether this effect is directionally stabilizing or not depends on the vortex strength and the orientation of the vortices and boundary layer separation lines around the forebody. It was found in the water tunnel that on the F-14 in sideslip, the leeward vortex is closest to the surface and near the side of the body while the windward vortex is higher above the surface and nearer the fuselage centerline. This vortex orientation in sideslip will change the circumferential pressure distribution over the forebody and so produce a net side force. The net side force is to the leeward side because the leeward vortex is the closest to the surface and therefore has the greatest influence. Since the side force acts on the leeward side, it will pull the forebody farther out of alignment with the freestream. This is an unstable yawing moment which will reduce the directional stability. In Figure 9 an unstable yawing moment is produced at 10° of sideslip and 30° angle of attack. By 30° angle of attack, the contribution of the forebody to the directional stability is the dominant effect.

CONCLUDING REMARKS

Flow visualization studies were conducted in the Northrop water tunnel to provide qualitative definition of the vortex flow fields occurring on the F-14 fighter aircraft configuration. Details of the glove and forebody vortex flow fields were obtained for angles of attack up to 55° at sideslip angles of 0° and 10°. The documentation covered the vortex flow field development, vortex path, and vortex breakdown characteristics. The water tunnel flow visualization is an aid in interpreting the results of wind tunnel tests. The high angle of attack stability characteristics measured in a wind tunnel have been correlated to the orientation and structure of the vortex flow fields. Many of the flow visualization results will provide guidance to NASA DFRC in planning future full-scale F-14 flight tests. A summary of the flow visualization results is given below and conclusions are made where appropriate:

1. Both a glove vortex and an inlet vortex were formed above the aircraft at zero sideslip. By 15° angle of attack, the glove and inlet vortices had combined into a single vortex above the glove. The burst point of the glove vortex moved forward and inboard with increasing angle of attack. The glove vortex breaks down completely above 30° angle of attack.

2. The vortices above the gloves shifted away from the windward side of the model in sideslip. The difference in strength between the vortices in sideslip, with the windward vortex increasing in strength, contributes to a stable rolling moment. The asymmetric breakdown of the vortices in sideslip at the higher angles of attack causes a reduction in lateral stability.

3. The shielding of the vertical tails by the fuselage and the immersion of the windward vertical tail into the low velocity wake of the burst windward vortex reduced the dynamic pressure at the vertical tails and resulted in a loss of directional stability. The windward vortex induces an adverse sidewash in the region of the windward vertical tail. This is an additional destabilizing effect.

4. A symmetrical vortex pair was formed above the upper surface of the forebody by 30° angle of attack. A large asymmetry had developed in the forebody vortices

by 55° angle of attack. The large nose boom generated a turbulent wake which was seen to reduce the asymmetry in the forebody vortices.

5. The directional stability characteristics at the higher angles of attack were influenced by the orientation of the forebody vortex system in sideslip. The circular cross-sectional shape of the forebody produces a vortex pattern in sideslip that would generate a destabilizing yawing moment throughout the high angle of attack range.

REFERENCES

1. Chambers, J. R. and Grafton, S. B., "Aerodynamic Characteristics of Airplanes at High Angles of Attack," NASA TM-74097, 1977.

2. Headley, J. W., "Analysis of Wind Tunnel Data Pertaining to High Angle-of-Attack Aynamics," AFFDL TR-78-94, Volume I, 1978.

3. Lorincz, D. J., "Water Tunnel Flow Visualization Study of the F-15," NASA CR-144878, 1978.

4. Erickson, G., "Water Tunnel Flow Visualization: Insight Into Complex Three-Dimensional Flow Fields," AIAA Paper 79-1530, July 1979.

5. Poisson-Quinton, Ph. and Werlé, H., "Water Tunnel Visualization of Vortex Flow," Astronautics and Aeronautics, June 1967.

6. Werlé, H., "Hydrodynamic Flow Visualization," Annual Review of Fluid Mechanics, Volume 5, pp. 361-382, 1973.

7. Bihrle, W. and Meyer, R., "F-14A Flight Characteristics at High Angles of Attack," AIAA Paper 75-170, January 1975.

8. Hummel, D., "Untersuchungen uber das Aufplatzen der Wirbel an schlanken Delta-flugeln," Z. Flugwiss. 13, pp. 158-168, 1965.

9. Carr, P. C. and Gilbert, W. P., "Effects of Fuselage Forebody Geometry on Low-Speed Lateral-Directional Characteristics of Twin-Tail Fighter Model at High Angles of Attack," NASA TP-1592, 1979.

10. Peake, D. J., Owen, F. K., and Johnson, D. A., "Control of Forebody Vortex Orientation to Alleviate Side Forces," AIAA Paper 80-0183, January 1980.

11. Lamont, P. J. and Hunt, B. L., "Pressure and Force Distributions on a Sharp-Nosed Circular Cylinder at Large Angles of Inclination to a Uniform, Subsonic Stream," Journal of Fluid Mechanics, Vol. 76, Part 3, pp. 519-559, 1976.

12. Keener, E.R. and Chapman, G.T., "Onset of Aerodynamic Side Forces at Zero Sideslip on Symmetric Forebodies at High Angles of Attack," AIAA Paper 74-770, August 1974.

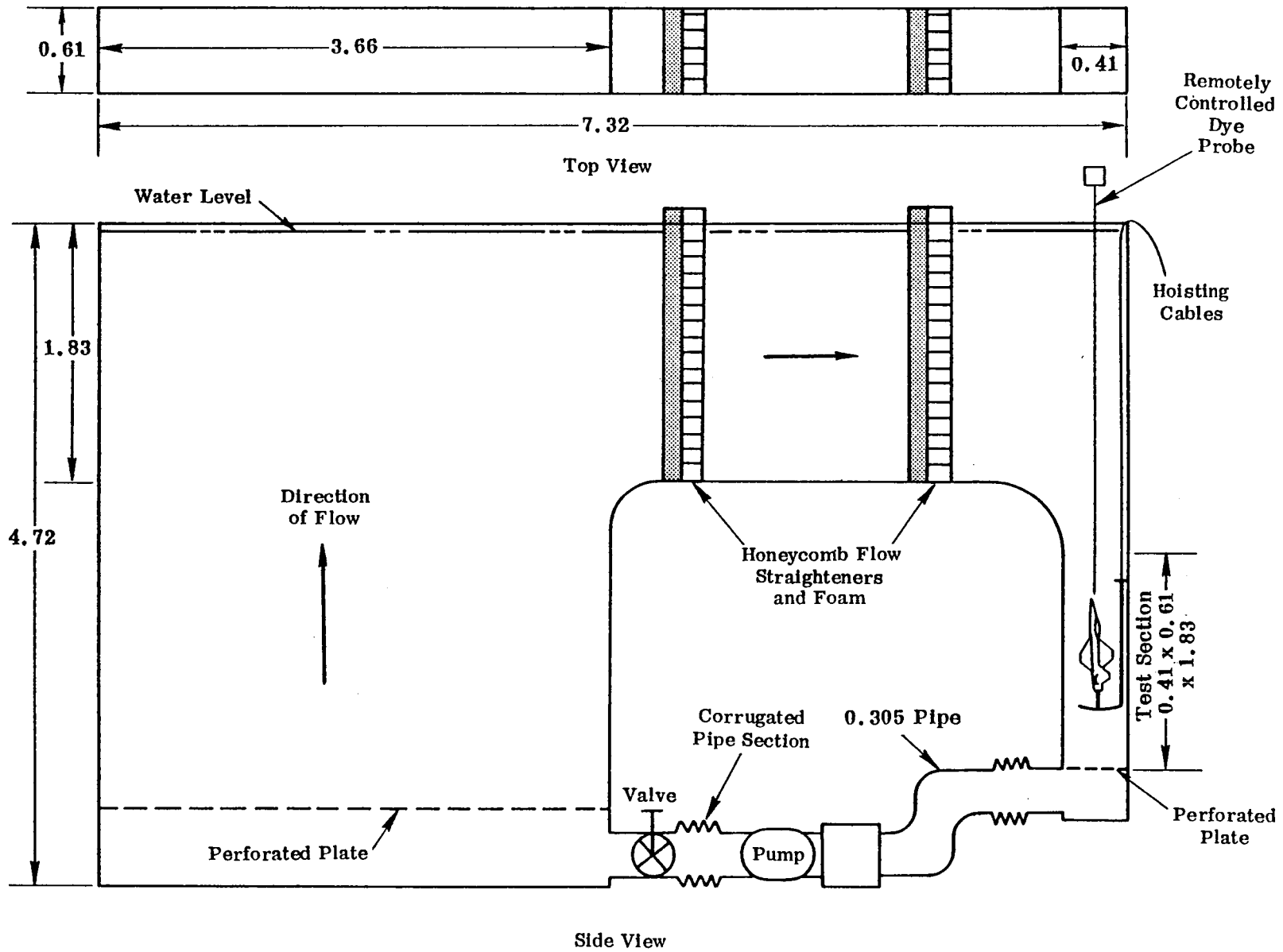

FIGURE 1. NORTHROP DIAGNOSTIC WATER TUNNEL (ALL DIMENSIONS IN M)

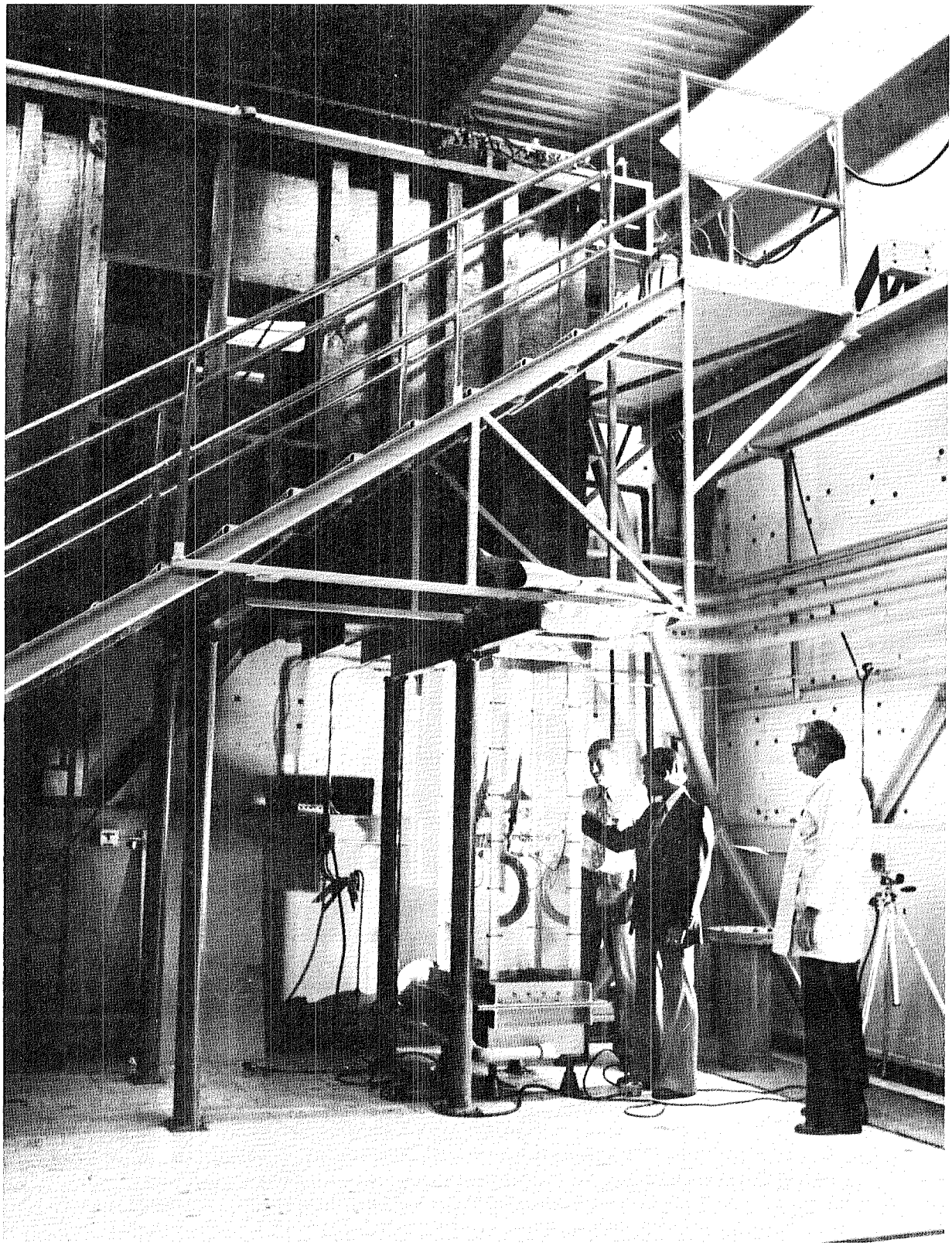

79-03669-7

FIGURE 2. MODEL INSTALLED IN WATER TUNNEL

		Facility (Method)	Reynolds No.
○	Northrop 16 x 24 in.	Water Tunnel (Dye)	$2.0(10^4)$
●	Northrop 6 x 6 in.	Water Tunnel (Dye)	$1.5(10^4)$
□	Wentz	Wind Tunnel (Schlieren)	10^6 (approx.)
◇	Poisson-Quinton & Erlich	Water Tank (Dye; aluminum Particles)	$2(10^4)$ (approx.)
△	Chigier	Wind Tunnel (Laser anemometer)	$2(10^6)$ (approx.)
▽	Earnshaw and Lawford	Wind Tunnel (Tuft probe)	(10^6) (approx.)
▲	Hummel and Srinivasan	Wind Tunnel (Smoke)	(10^6) (approx.)
☆	Lowson	Water Tunnel (Dye)	$3(10^4)$

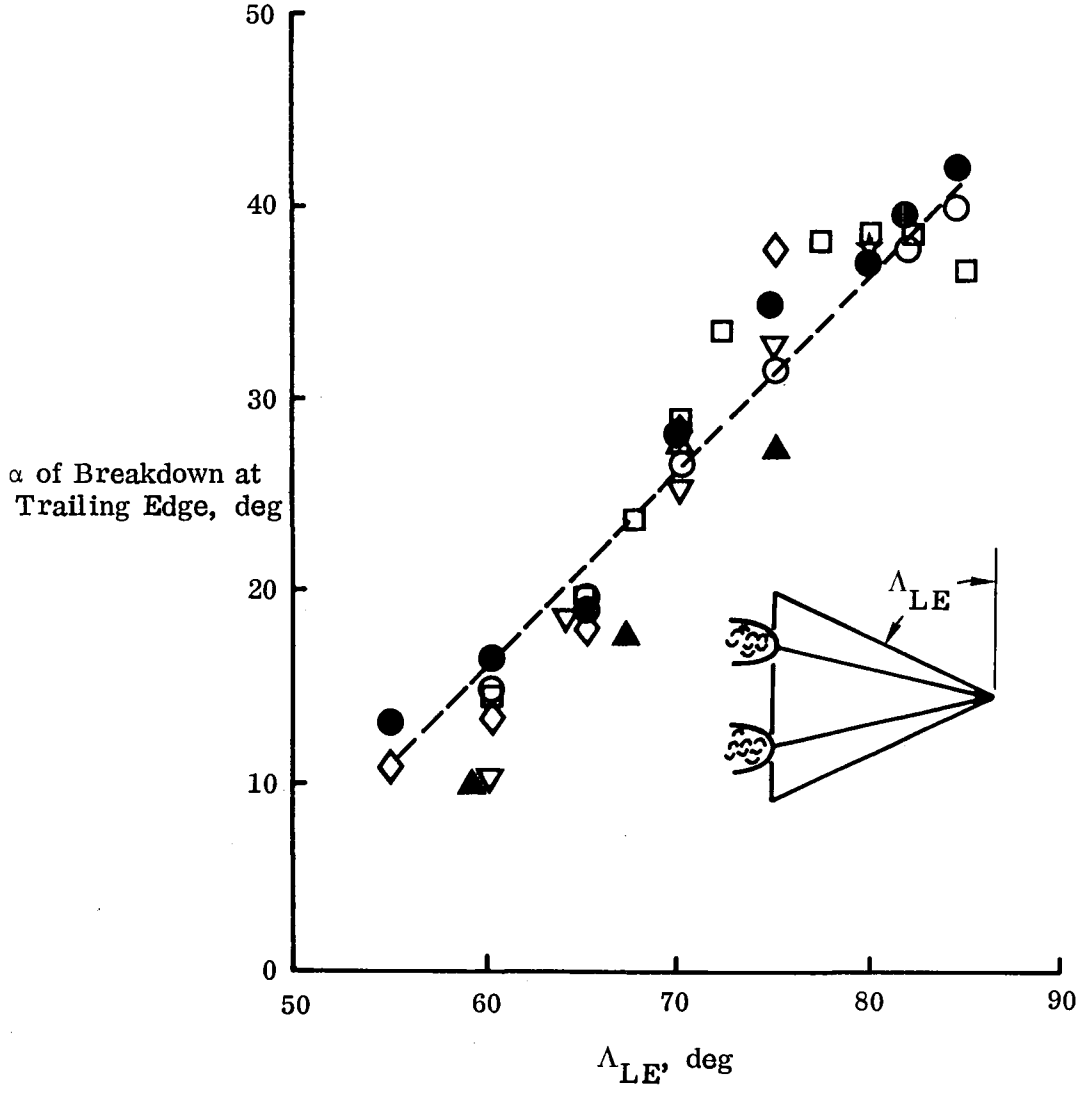

FIGURE 3. EFFECT OF LEADING-EDGE SWEEP ON THE ANGLE OF ATTACK OF VORTEX BREAKDOWN AT THE TRAILING EDGE OF DELTA WINGS (DATA FROM REFERENCE 4)

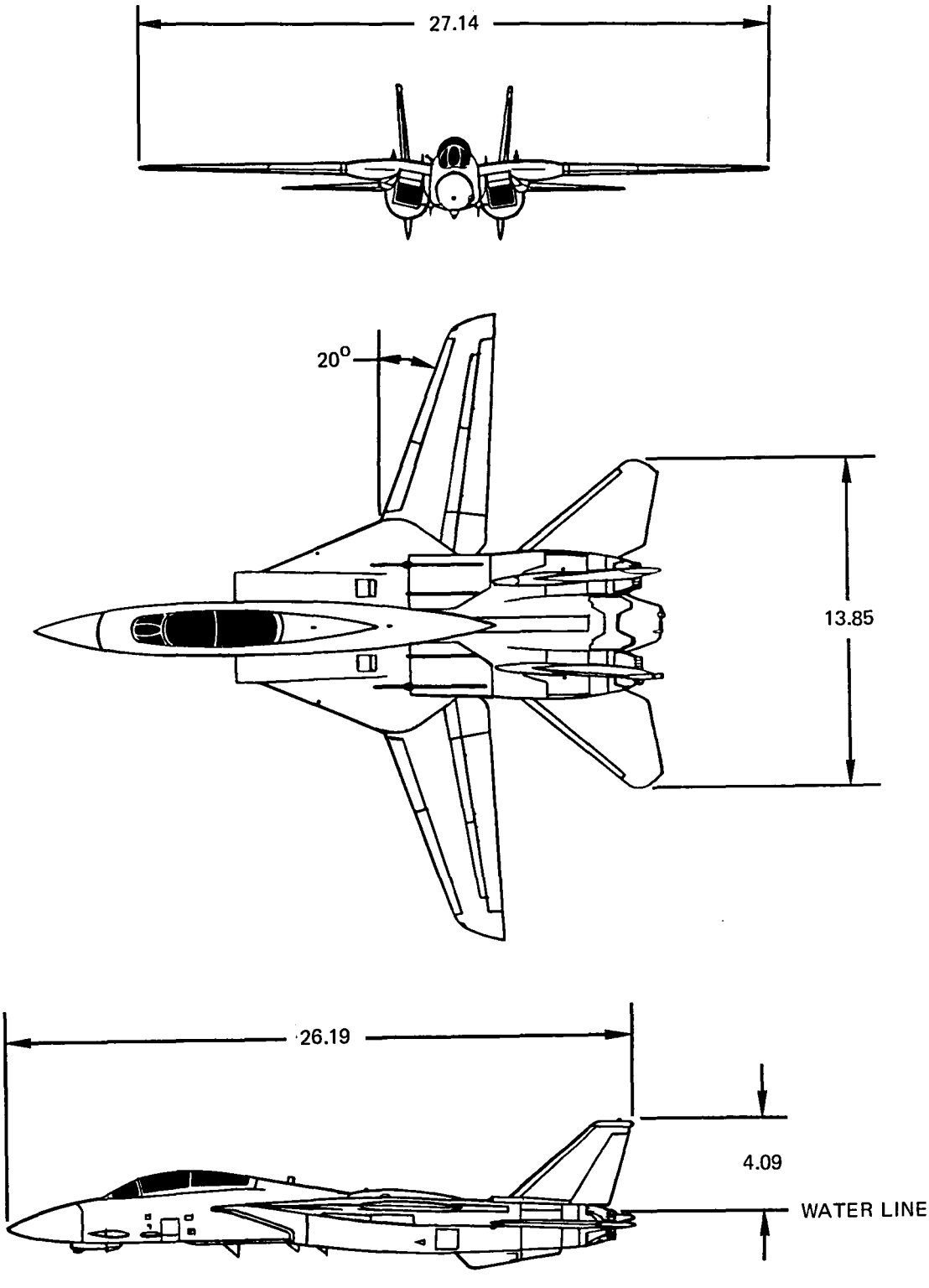

FIGURE 4. 1/72-SCALE F-14 MODEL THREE VIEW DRAWING
(ALL DIMENSIONS IN CM)

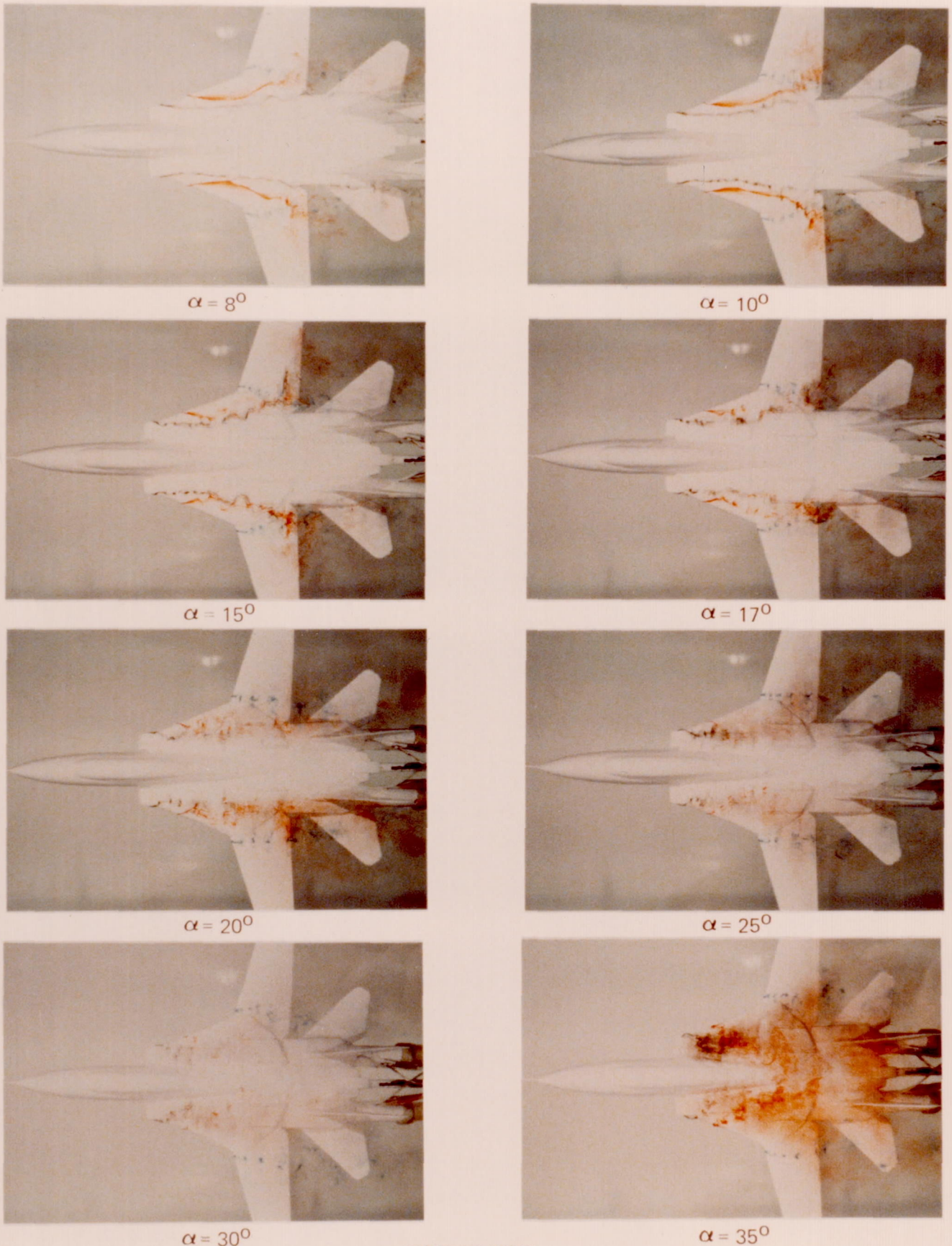

(A) PLAN VIEW

FIGURE 5. WING-GLOVE FLOW FIELD FOR $\beta = 0^{\circ}$

$\alpha = 8^{o}$

$\alpha = 10^{o}$

$\alpha = 15^{o}$

$\alpha = 17^{o}$

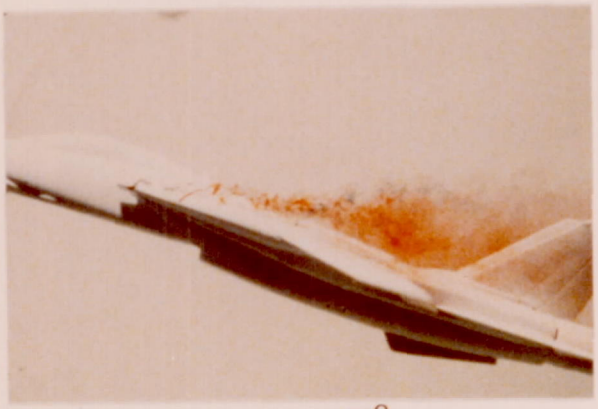

$\alpha = 20^{o}$

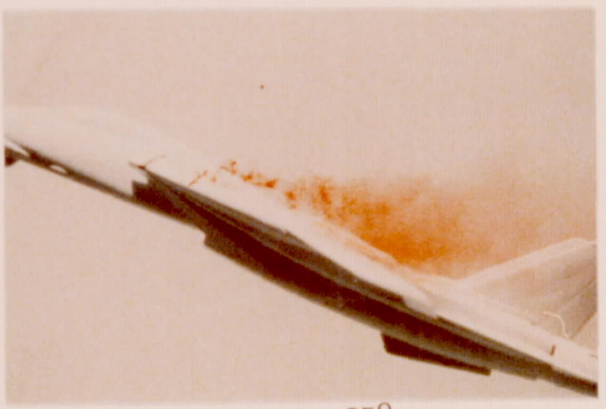

$\alpha = 25^{o}$

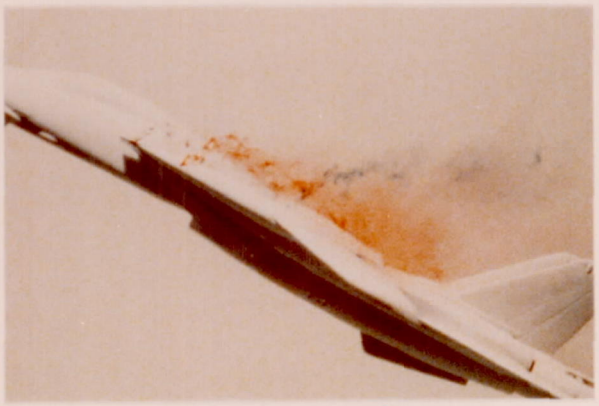

$\alpha = 30^{o}$

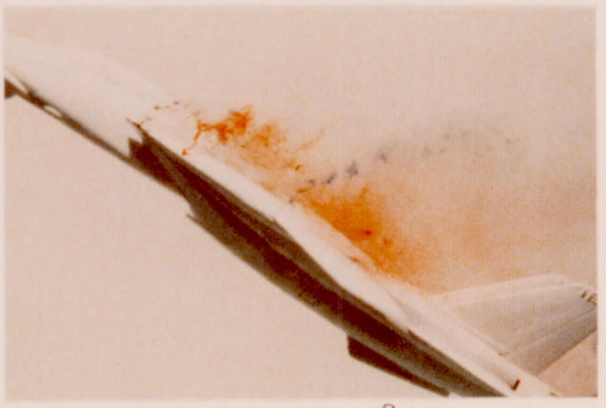

$\alpha = 35^{o}$

(B) PROFILE VIEW

FIGURE 5. CONCLUDED

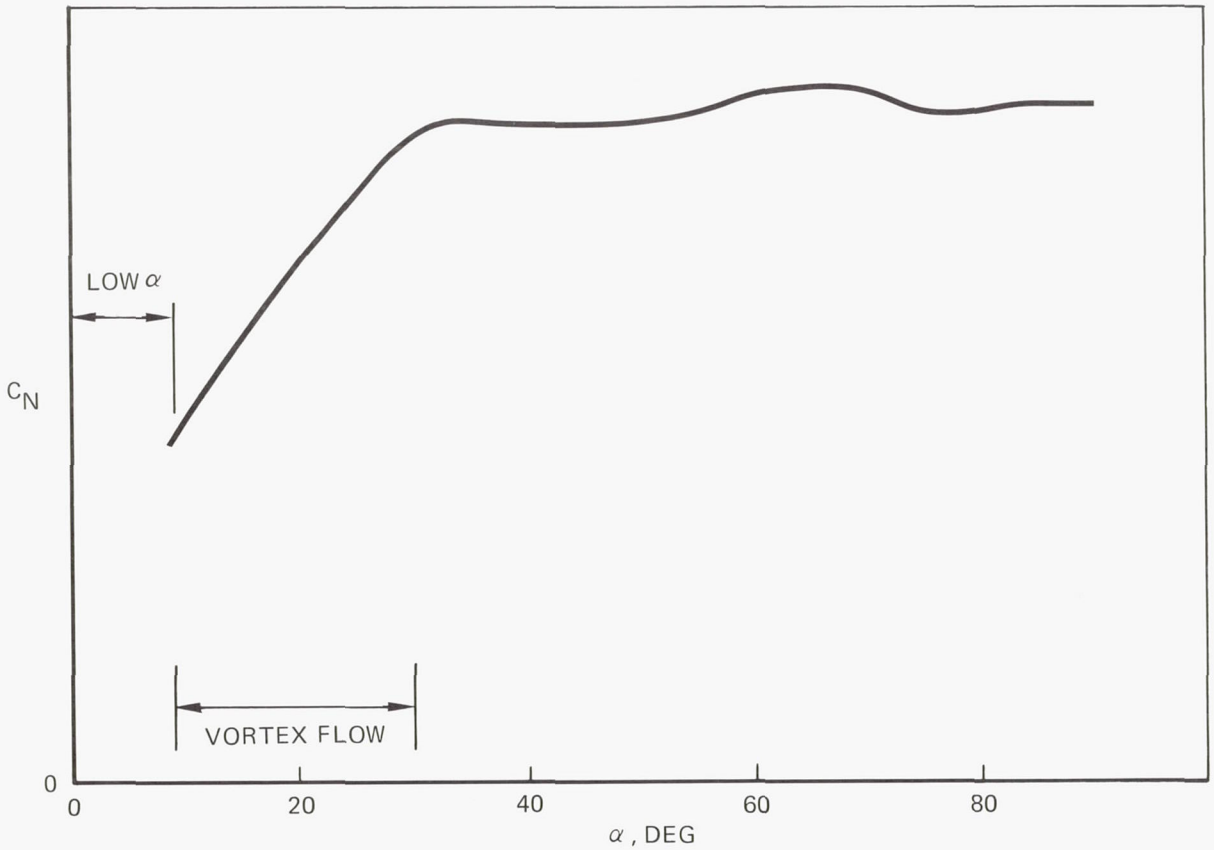

FIGURE 6. LOW-SPEED NORMAL FORCE CHARACTERISTICS OF THE F-14, $\Lambda = 22^{o}$ (DATA FROM REFERENCE 7)

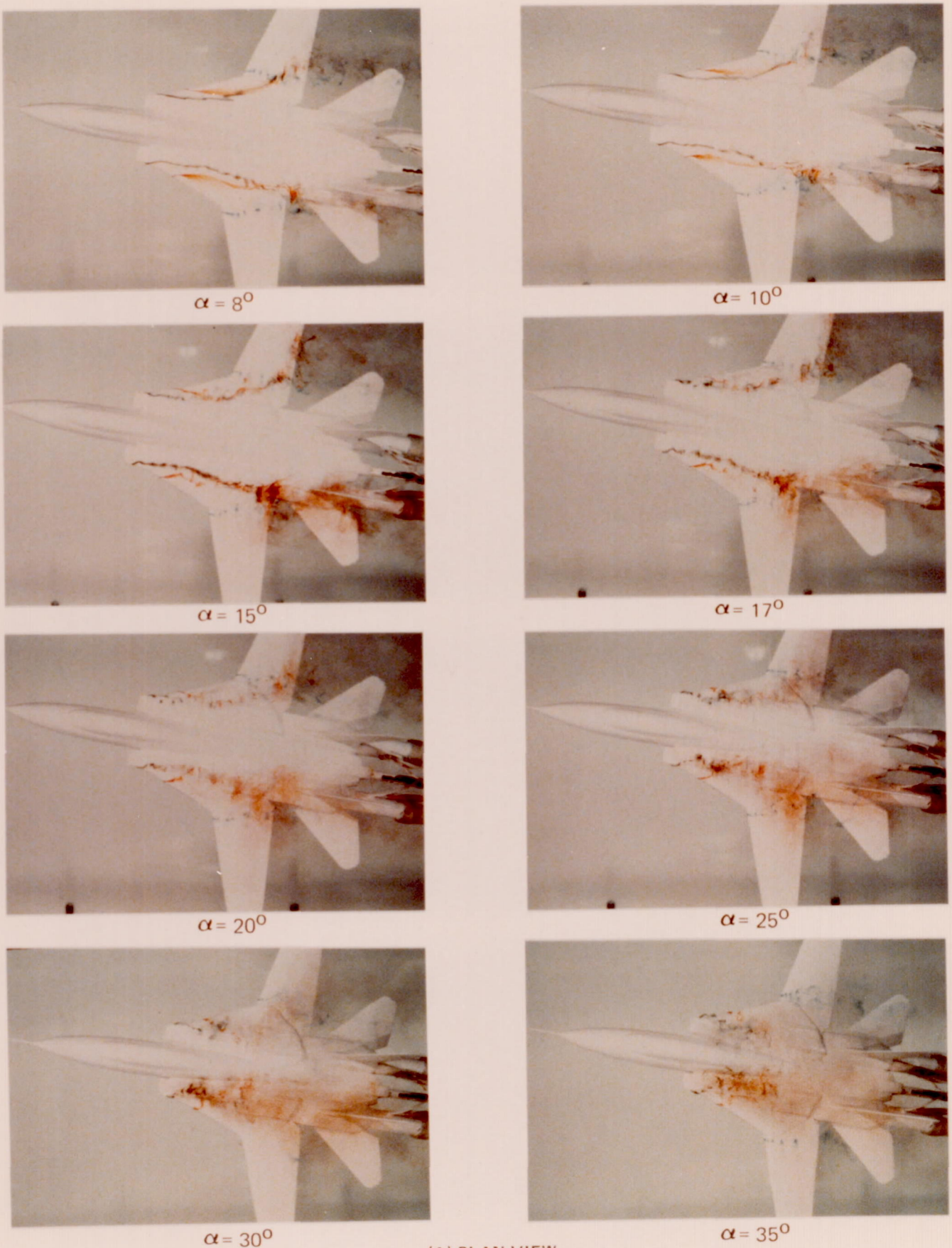

(A) PLAN VIEW

FIGURE 7. EFFECT OF SIDESLIP ON WING-GLOVE FLOW FIELD, $\beta = 10^{o}$

$\alpha = 8^{o}$

$\alpha = 10^{o}$

$\alpha = 15^{o}$

$\alpha = 17^{o}$

$\alpha = 20^{o}$

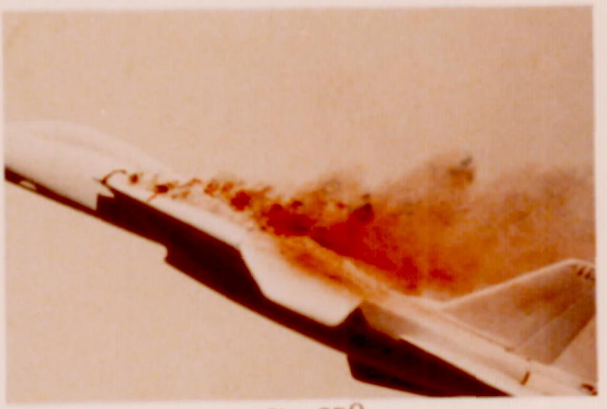

$\alpha = 25^{o}$

$\alpha = 30^{o}$

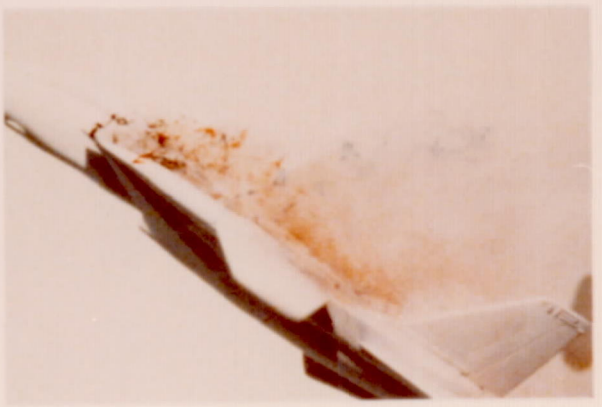

$\alpha = 35^{o}$

(B) WINDWARD PROFILE VIEW

FIGURE 7. CONCLUDED

FIGURE 8. FLOW FIELD NEAR VERTICAL TAILS FOR $\alpha = 20^{o}$, $\beta = -10^{o}$

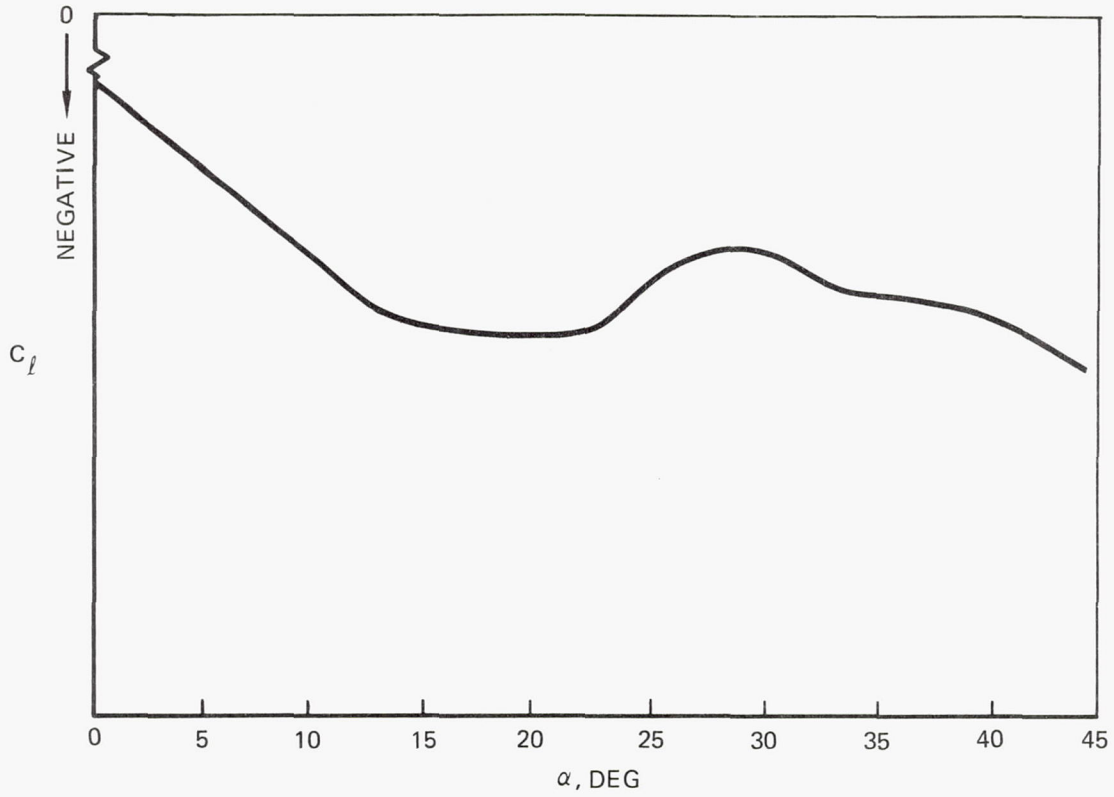

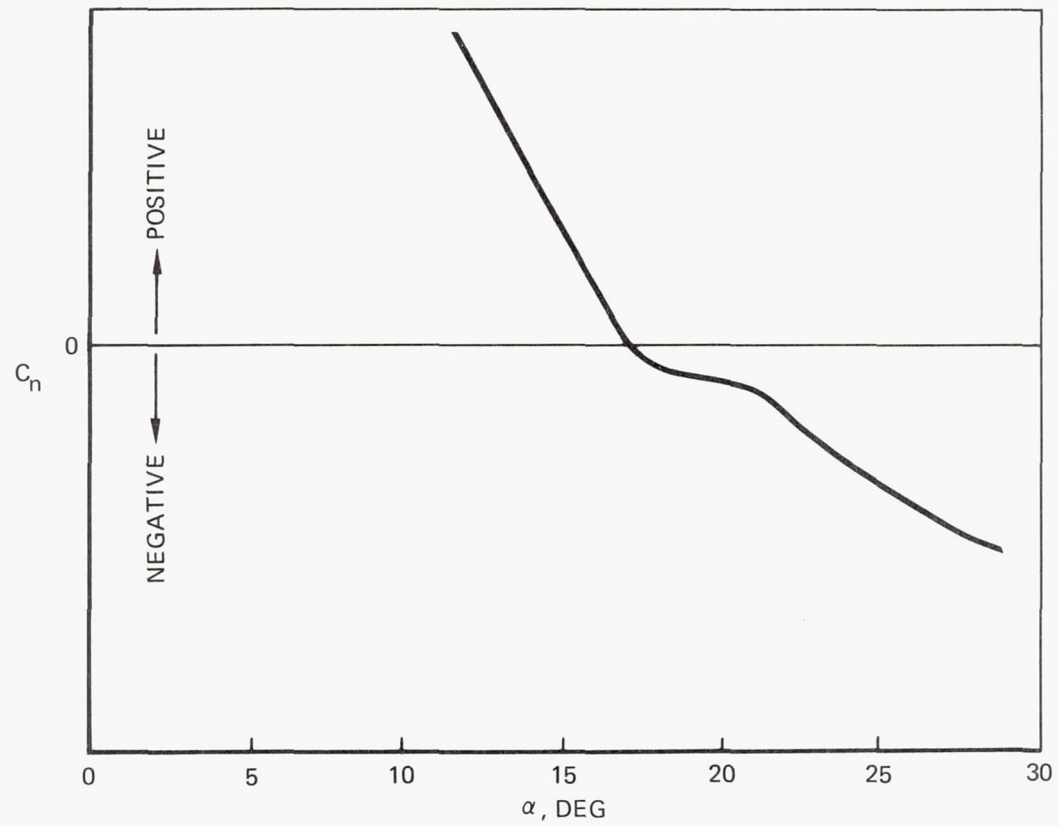

FIGURE 9. LATERAL/DIRECTIONAL CHARACTERISTICS OF THE F-14 FOR $M = 0.2, \beta = 10^{o}, \Lambda = 22^{o}$ (DATA FROM REFERENCE 7)

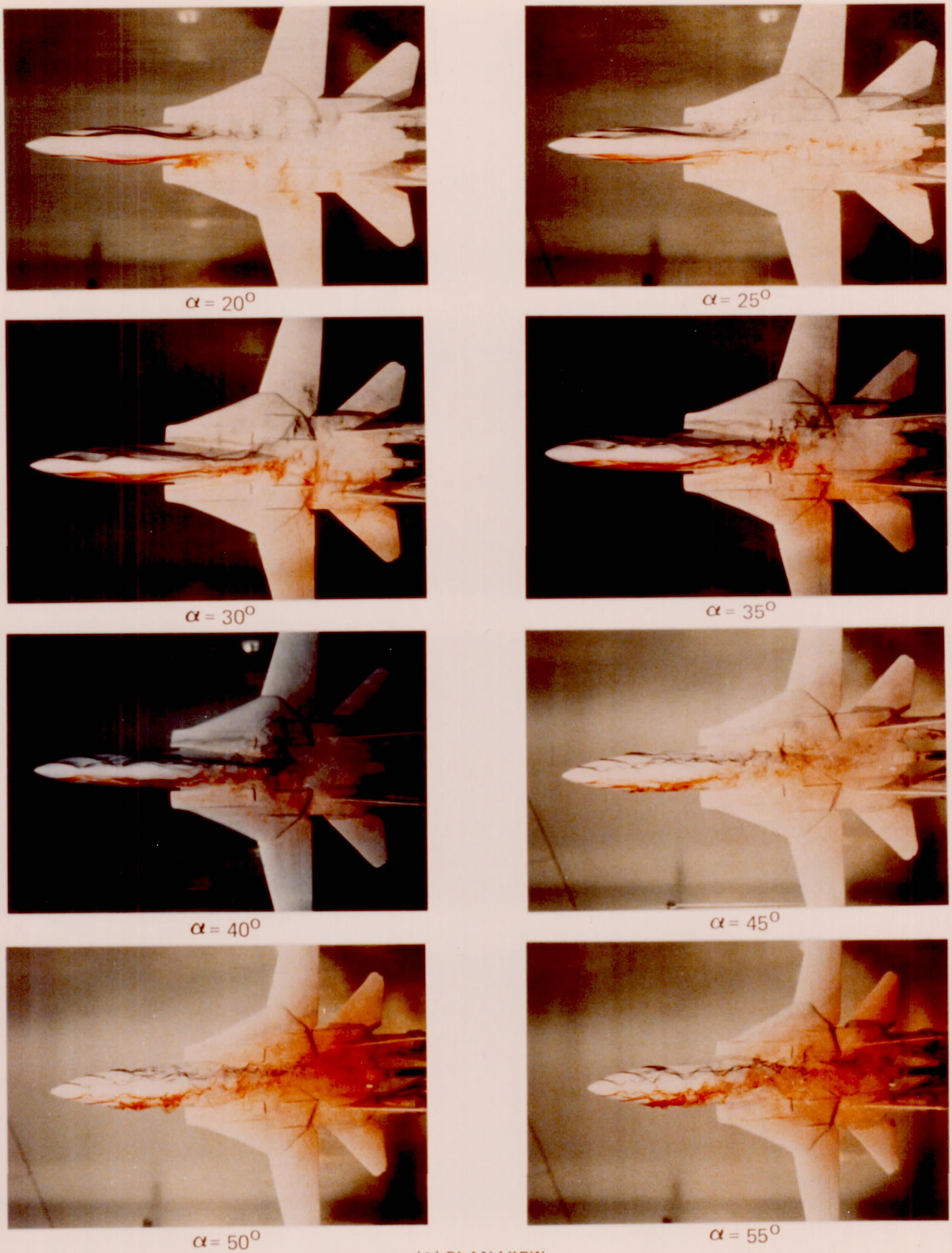

(A) PLAN VIEW

FIGURE 10. FOREBODY FLOW FIELD FOR $\beta = 0^{o}$

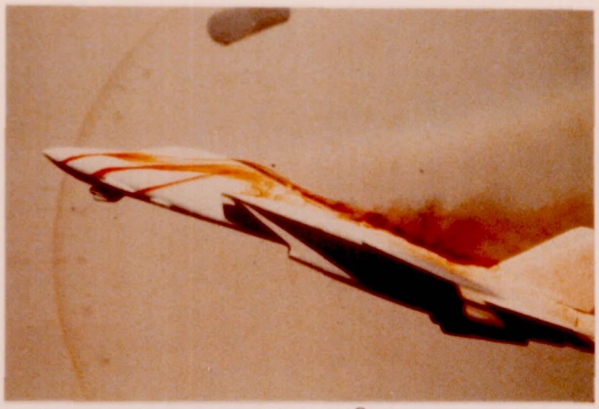

$\alpha = 20^{o}$

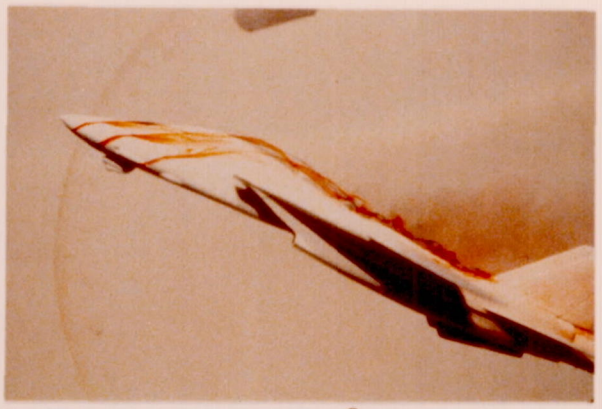

$\alpha = 25^{o}$

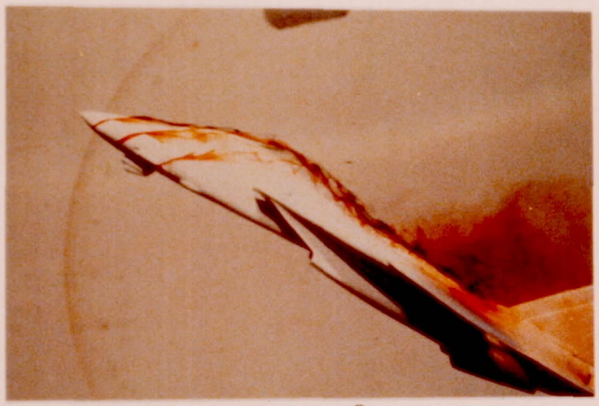

$\alpha = 30^{o}$

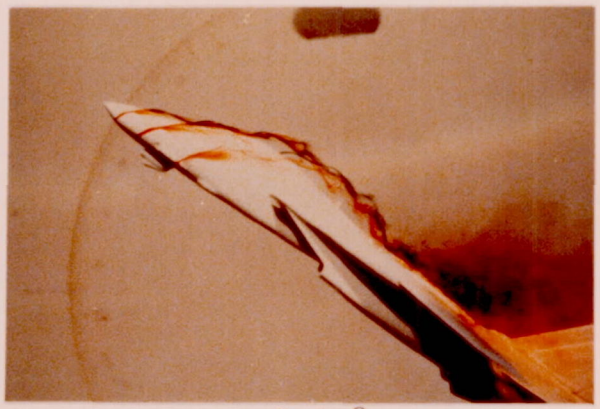

$\alpha = 35^{o}$

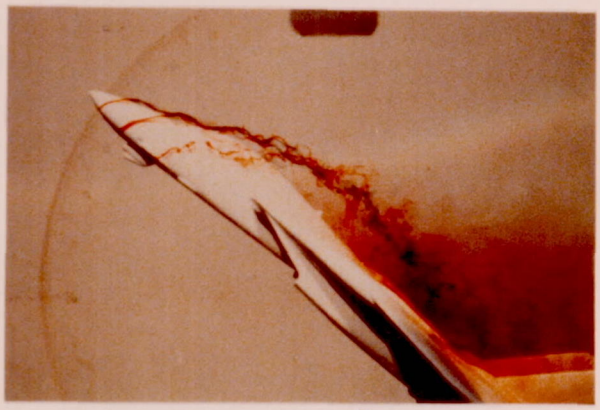

$\alpha = 40^{o}$

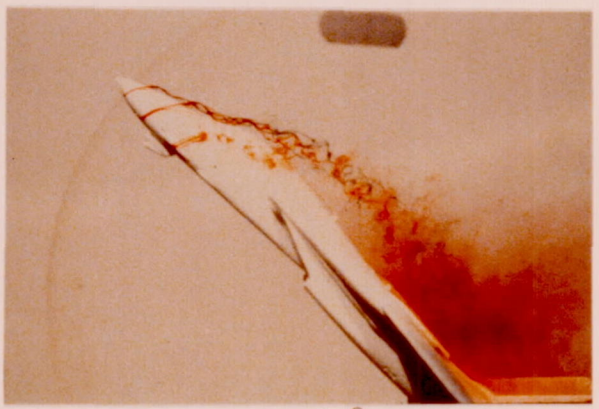

$\alpha = 45^{o}$

$\alpha = 50^{o}$

$\alpha = 55^{o}$

(B) PROFILE VIEW

FIGURE 10. CONCLUDED

(A) PLAN VIEW

FIGURE 11. EFFECT OF NOSE BOOM ON FOREBODY FLOW FIELD FOR $\beta = 0^{o}$

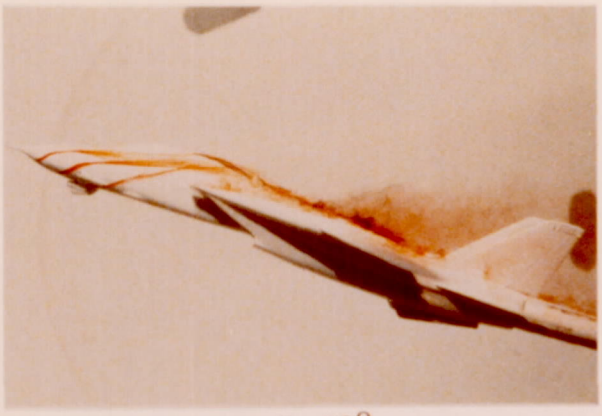

$\alpha = 20^{o}$

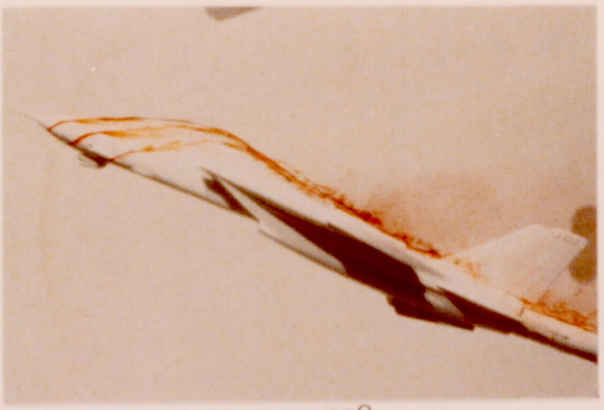

$\alpha = 25^{o}$

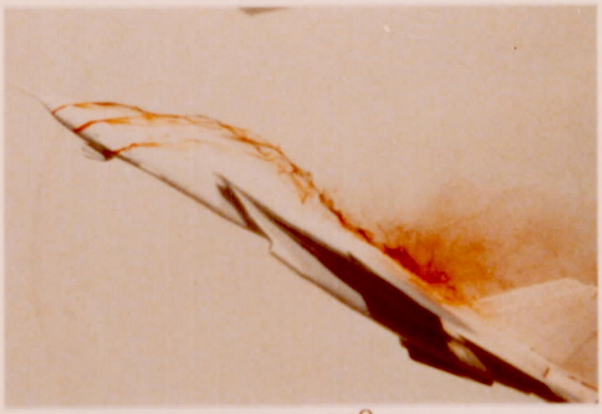

$\alpha = 30^{o}$

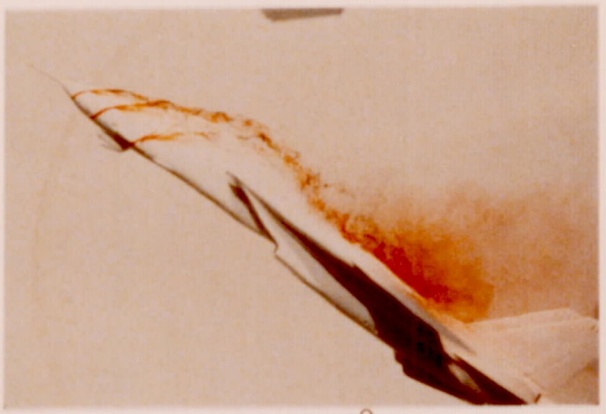

$\alpha = 35^{o}$

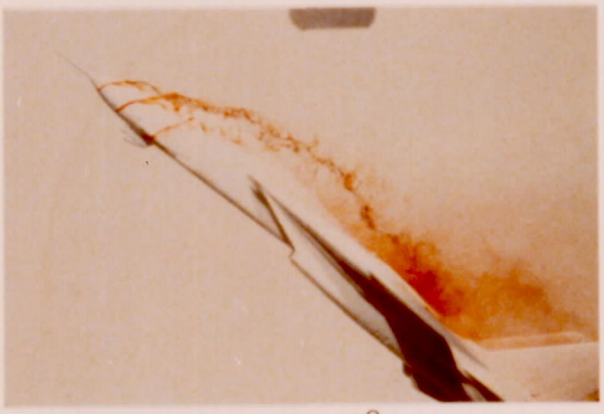

$\alpha = 40^{o}$

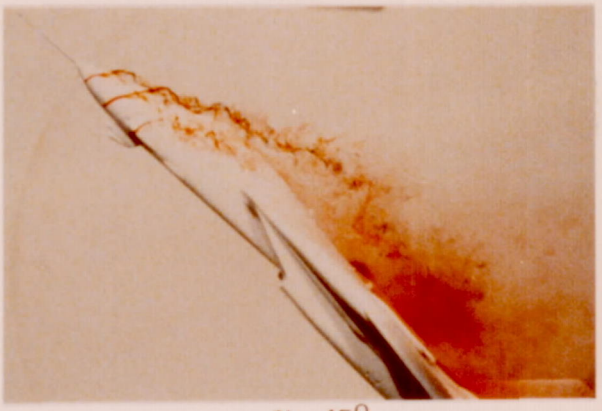

$\alpha = 45^{o}$

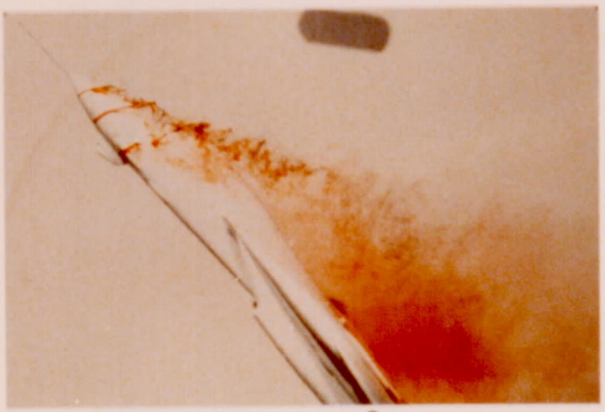

$\alpha = 50^{o}$

$\alpha = 55^{o}$

(B) PROFILE VIEW

FIGURE 11. CONCLUDED

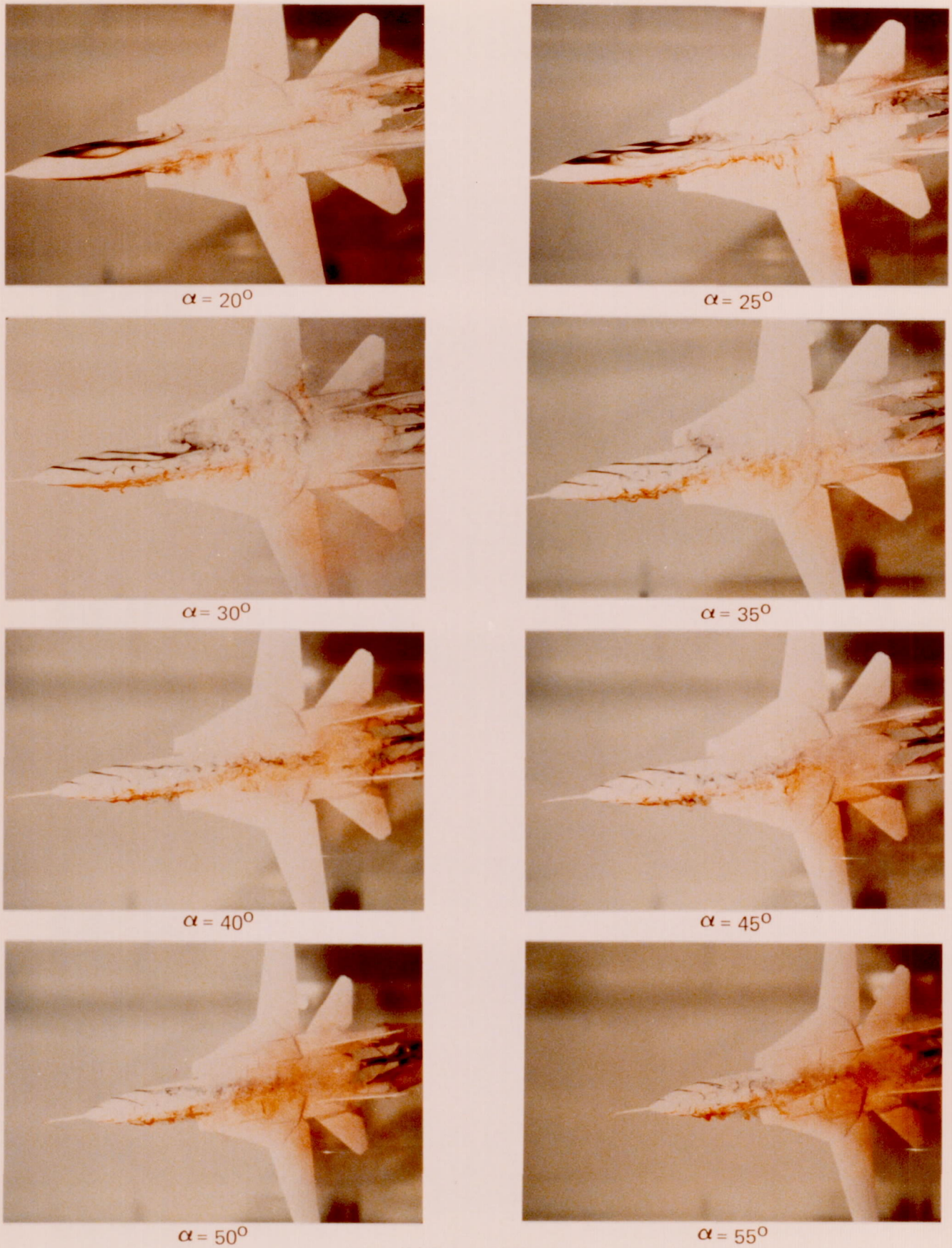

(A) PLAN VIEW

FIGURE 12. EFFECT OF SIDESLIP ON FOREBODY FLOW FIELD, $\beta = 10^{o}$

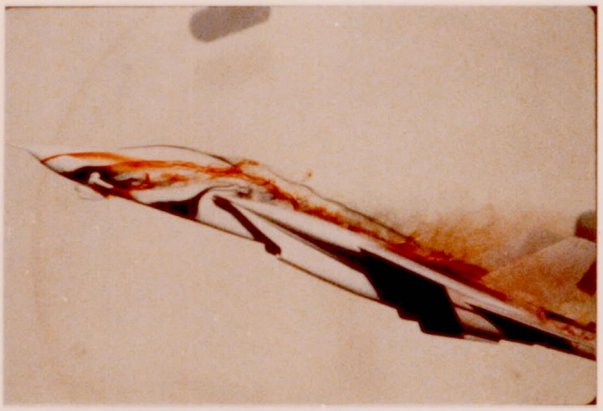

$\alpha = 20^{o}$

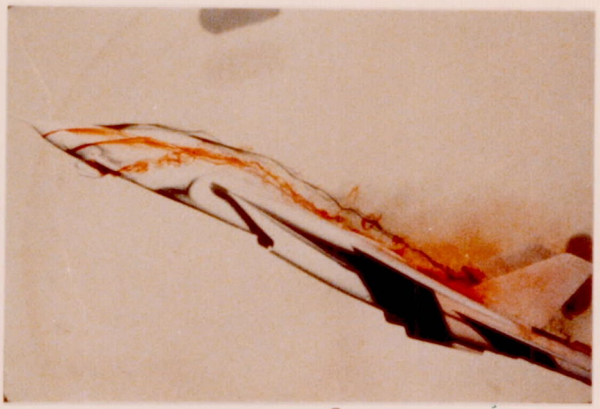

$\alpha = 25^{o}$

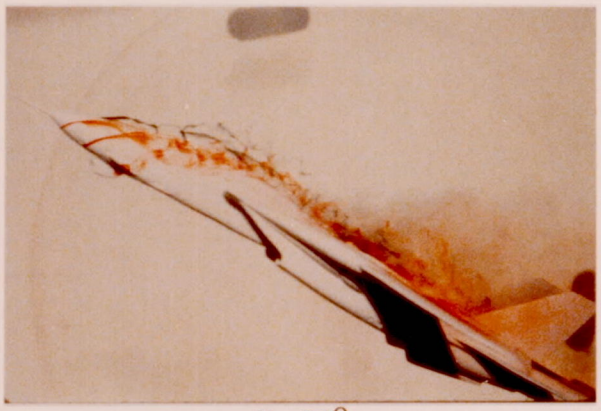

$\alpha = 30^{o}$

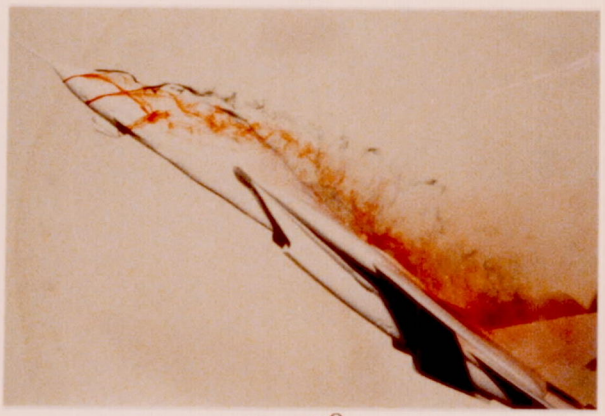

$\alpha = 35^{o}$

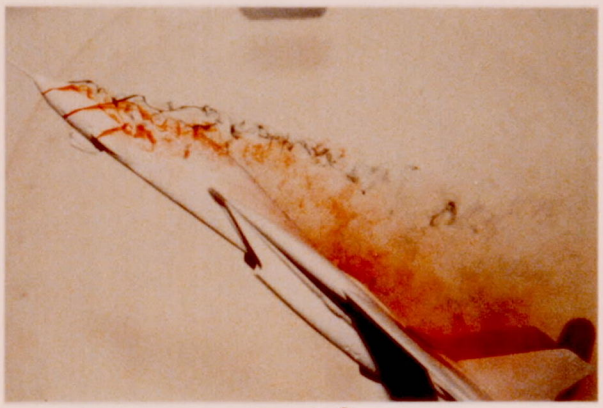

$\alpha = 40^{o}$

$\alpha = 45^{o}$

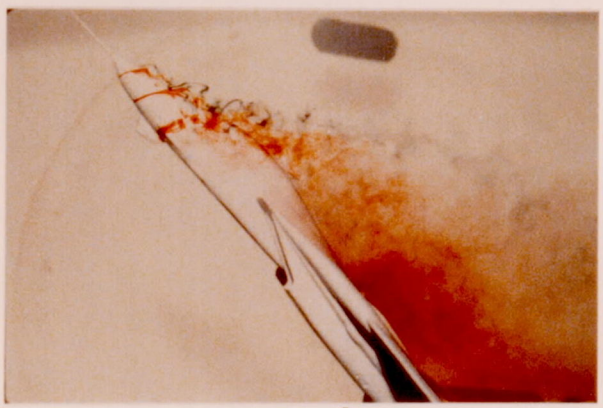

$\alpha = 50^{o}$

$\alpha = 55^{o}$

(B) LEEWARD PROFILE VIEW

FIGURE 12. CONTINUED

$\alpha = 20^{o}$

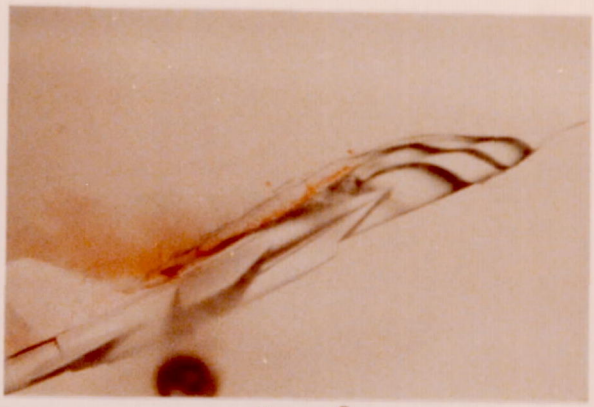

$\alpha = 25^{o}$

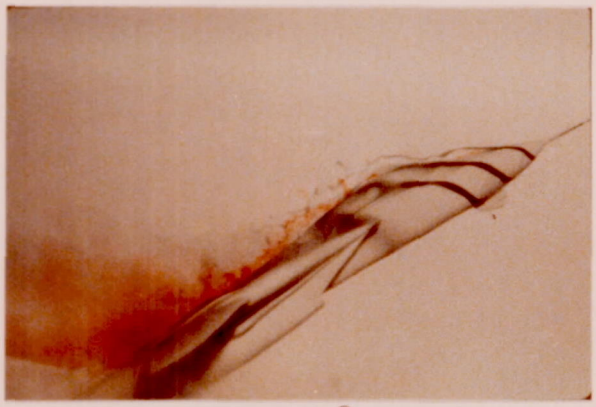

$\alpha = 30^{o}$

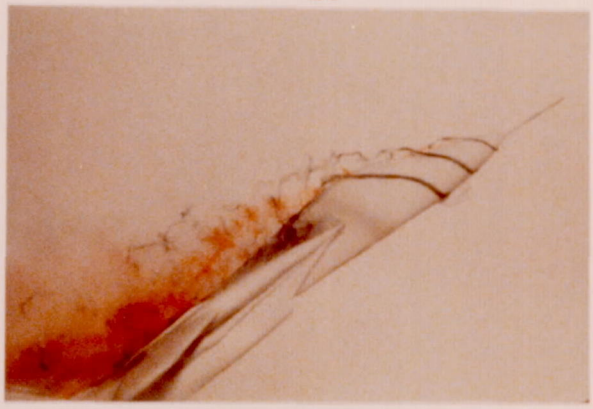

$\alpha = 35^{o}$

$\alpha = 40^{o}$

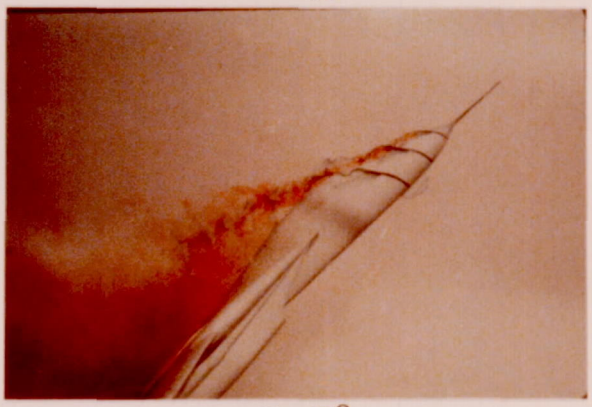

$\alpha = 45^{o}$

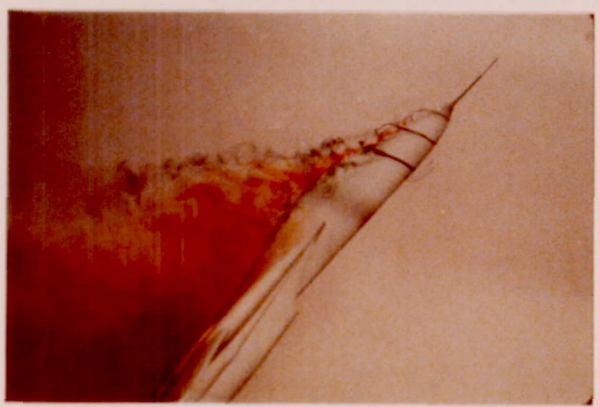

$\alpha = 50^{o}$

$\alpha = 55^{o}$

(C) WINDWARD PROFILE VIEW

FIGURE 12. CONCLUDED

1. Report No.	2. Government Accession No.	3. Recipient's Catalog No.
NASA CR-163098		

4. Title and Subtitle	5. Report Date
FLOW VISUALIZATION STUDY OF THE F-14 FIGHTER AIRCRAFT CONFIGURATION	September 1980
	6. Performing Organization Code

7. Author(s)	8. Performing Organization Report No.
Dale J. Lorincz	NOR 80-150
	10. Work Unit No.

9. Performing Organization Name and Address	11. Contract or Grant No.
Northrop Corporation Aircraft Division 3901 West Broadway Hawthorne, California 90250	NAS4-2616
	13. Type of Report and Period Covered
12. Sponsoring Agency Name and Address	Contractor Report - Topical
National Aeronautics and Space Administration Washington, D.C. 20546	14. Sponsoring Agency Code H-1135

15. Supplementary Notes

NASA Technical Monitor: Edward L. Friend, Dryden Flight Research Center

16. Abstract

Water tunnel studies have been performed to qualitatively define the flow field of the F-14. Particular emphasis was placed on defining the vortex flows generated at high angles of attack. The flow visualization tests were conducted in the Northrop water tunnel using a 1/72-scale model of the F-14 with a wing leading-edge sweep of 20°. Flow visualization photographs were obtained for angles of attack up to 55° and sideslip angles up to 10°.

The F-14 model was investigated to determine the vortex flow field development, vortex path, and vortex breakdown characteristics as a function of angle of attack and sideslip. Vortex flows were found to develop on the highly swept glove and on the upper surface of the forebody. At 10° of sideslip, the windward glove vortex shifted inboard and broke down farther forward than the leeward glove vortex. This asymmetric breakdown of the vortices in sideslip contributes to a reduction in the lateral stability above 20° angle of attack. The initial loss of directional stability is a consequence of the adverse sidewash from the windward vortex and the reduced dynamic pressure at the vertical tails.

Asymmetries in the forebody vortex system were observed in the water tunnel at zero sideslip and high angles of attack. A large nose boom was added to the forebody and was seen to shed a turbulent wake which reduced the vortex asymmetry. The orientation of the forebody vortex system in sideslip was found to influence the directional stability at high angles of attack.

17. Key Words (Suggested by Author(s))	18. Distribution Statement
High angle of attack aerodynamics Lateral/directional stability Vortex flow fields Forebody effects Water tunnel flow visualization	Unclassified - Unlimited Subject category: 02

19. Security Classif. (of this report)	20. Security Classif. (of this page)	21. No. of Pages	22. Price
Unclassified	Unclassified	40	

* *For sale by the National Technical Information Service, Springfield, Virginia 22161*

End of Document